Energy dependence of experimental Be Compton profiles

S. Huotari, K. Hämäläinen, and S. Manninen
Department of Physics, P.O. Box 9, FIN-00014 University of Helsinki, Helsinki, Finland

S. Kaprzyk* and A. Bansil
Department of Physics, Northeastern University, Boston, Massachusetts 02115

W. Caliebe
Institut für Festkörperforschung, FZ Jülich, 52425 Jülich, Germany

T. Buslaps, V. Honkimäki, and P. Suortti
European Synchrotron Radiation Facility, Boîte Postale 220, F-38043 Grenoble Cedex, France
(Received 10 December 1999)

High-resolution Compton scattering measurements on Be single crystals along three main crystallographic directions ([10·0], [11·0], and [00·1]) have been carried out using incident photon energies of 10, 29, and 56 keV to study the energy dependence of the scattering cross section. The experimental Compton profiles are in good agreement with theoretical profiles employing the local density approximation–based band theory framework. Extensive comparisons between the computed and measured profiles, their first derivatives, and anisotropies defined as differences between various pairs of profiles show an excellent level of accord. The details related to the Fermi surface are clearly seen in the experimental Compton profiles. However, subtle but systematic direction-dependent discrepancies remain between the experimental and theoretical profiles, suggesting that a better treatment of electron correlation effects in the inhomogeneous electron gas is needed to develop a satisfactory description of the momentum density in Be. Our analysis also indicates that the effective momentum resolution in low-energy Compton experiments possesses intrinsic limitations due to final-state interactions and possibly cannot be enhanced arbitrarily by improving the instrumental resolution.

I. INTRODUCTION

Compton scattering, i.e., inelastic scattering of x rays at high momentum transfer, is an excellent tool for investigating the ground-state electronic properties of matter.[1–3] The technique is insensitive to crystal defects, yields information on the bulk properties, and does not require low temperatures. These advantages have made Compton scattering well suited for studying the Fermi character of ordered as well as disordered materials. The development of spectrometers at the second and third generation synchrotron radiation facilities has made it possible now to achieve momentum resolution of the order of 0.1 a.u. in wide classes of materials and of the order of 0.01 a.u. in low-Z systems, while still preserving a high statistical accuracy.

Recent Compton work has indicated that the local density approximation (LDA)–based band theory framework is not adequate for describing a number of key aspects of the momentum density of the electron gas in metals and alloys.[4–9] The so-called Compton profile, used commonly to compare theory and experiment, is defined within the impulse approximation (IA),[10] which assumes that the potential experienced by the ejected electron is unchanged during the scattering process. The Compton profile can then be factorized from the measured scattering cross section. The IA is valid when the energy transferred to the recoil electron is significantly larger than its binding energy. The Compton spectrometers having the best momentum resolution typically operate at about 10 keV, which means that the energy transferred to the Compton electron is of the order of 1 keV, i.e., of the same order of magnitude as the binding energies of inner-shell electrons of light elements. Under these conditions the IA is not valid for the core electrons. In most cases the main interest is in the valence electrons, but in order to isolate the valence contribution, the core electron part must be known accurately. There are various approaches to make an ''exact'' calculation[11–15] but the experimental verification is very difficult. It is possible to separate the contribution of a particular electron shell from the Compton scattering cross section by using a coincidence technique, where the scattered photon is measured in coincidence with the fluorescence photon emitted when the vacancy left by the recoil electron is filled.[16,17] All these experiments have been made using low momentum resolution (0.6 a.u. or worse). The only high-resolution measurement has been made by Issolah *et al.*[11] using 8.2-keV and 12.86-keV photons. It should also be noted that in a Compton experiment one measures essentially a one-dimensional projection of the electron momentum density onto the direction of the scattering vector of the photon, so that structural details in the momentum density in the plane perpendicular to the scattering vector are not well-resolved. Nevertheless, by making Compton measurements along a number of different directions, the underlying three-dimensional momentum density may be reconstructed.[6,7,18,19]

Both the Fermi surface characterization and electron correlation studies have been particularly attractive applications

for high-resolution Compton scattering experiments.[4–9,20–22] The resolution of the order of 0.1 a.u. or better is generally adequate for delineating Fermi surface features in the spectra. One obvious feature is the sharp discontinuity in the momentum density in a metal at the Fermi momentum p_F. Recent Compton studies in a number of cases indicate that the observed Fermi break at p_F is broader and exhibits a larger high-momentum tail than expected to account for the effects of the lattice potential and the experimental resolution.[4–9,20–22] These results suggest the need for treating the electron correlation effects beyond the LDA in order to explain the Compton data. The observation of the Fermi break and the correlation smearing is possible only if the resolution is good enough and the shape of the resolution function is well characterized. Similar information can in principle be obtained by using positron annihilation spectroscopy,[23] where the resolution is comparable to that of the Compton spectrometers, but the involvement of the positron entangles the electron-electron with electron-positron correlation and complicates the interpretation of the spectra. Careful comparisons between the high-resolution positron annihilation and Compton measurements may provide interesting possibilities for separating the electron-electron from electron-positron effects.[24]

In order to gain insight into the aforementioned problems, the present article reports an extensive Compton study on Be single crystals. This choice was motivated by the fact that Be is well suited to investigate the valence as well as the core electron contribution, since it contains only two electrons of each kind. Furthermore, the band structure is well known, and the Fermi surface contains a number of structures (referred to as ''cigars'' and ''coronets''), providing a good testing ground for comparing theory and experiment. Three sets of Compton measurements using different photon energies and momentum resolutions (10 keV at a resolution of 0.02 a.u., 29 keV at 0.08 a.u., and 56 keV at 0.16 a.u.) have been carried out. The results provide a systematic study of the effects of momentum resolution on the observability of fine structure in the Compton spectra.

II. THEORY

The theory of Compton scattering is well known (see, e.g., Ref. 25). The cross section for a photon with energy E_1 to be Compton scattered to energy E_2 in the IA can be written as

$$\frac{d^2\sigma}{d\Omega dE_2} = C(E_1, E_2, \phi) J(p_z), \tag{2.1}$$

where $C(E_1, E_2, \phi)$ is a function that depends on the experimental setup, while the properties of the electronic system under study are separated into the Compton profile $J(p_z)$, which is related to the momentum density $N(\mathbf{p})$ of the electron gas via a two-dimensional (2D) integral in a plane perpendicular to the direction of the scattering vector,

$$J(p_z) = \int\int N(\mathbf{p}) dp_x dp_y . \tag{2.2}$$

Equations (2.1) and (2.2) make it clear that Compton spectroscopy provides a direct probe of the ground-state wave function via the momentum density $N(\mathbf{p})$. The effects of the electron-electron correlation on the momentum density of the homogeneous electron gas have been investigated extensively for many decades using a variety of approximation schemes[26–32] but less so in the inhomogeneous case. Lam and Platzman[33] proposed a way to incorporate the correlation effects into the inhomogeneous electron gas. They also give a series of useful approximation schemes, where one of the most often used is based on the local density approximation. Correlations move some of the momentum density from below to above the Fermi energy, while the break in the occupation number at the Fermi momentum persists but gets renormalized to a smaller value $Z_F < 1$. The value of Z_F increases with increasing electron density as the kinetic energy dominates. Beyond this, the specific value of Z_F for a given electron density shows a substantial spread between various theoretical models. These key theoretical predictions should be amenable to experimental verification via high-resolution Compton scattering experiments, and as a result, the subject is drawing renewed theoretical interest.[34–37]

The case when the recoil electron is not scattered far enough in energy and momentum, so that the Compton limit is not satisfied, deserves some comment. The essential physics may be exposed with reference to the homogeneous electron gas for simplicity. The associated occupation number $n(\mathbf{p})$ can be written at $T=0$ as (see, e.g., Ref. 38)

$$n(\mathbf{p}) = \int_{-\infty}^{\mu} \frac{d\epsilon}{2\pi} A(\mathbf{p}, \epsilon), \tag{2.3}$$

where μ denotes the chemical potential. $A(\mathbf{p}, \epsilon)$ is the spectral density of the one-electron Green's function,

$$A(\mathbf{p}, \epsilon) = -2 \,\mathrm{Im}\, G(\mathbf{p}, \epsilon). \tag{2.4}$$

The occupation number $n(\mathbf{p})$ and the momentum density $N(\mathbf{p})$ must be distinguished here. For a homogeneous electron gas, the only difference between these two is a normalization constant, since the momentum density $N(\mathbf{p})$ in Eq. (2.2) is normalized so that $\int_{-\infty}^{\infty} J(p_z) = Z$, but $n(\mathbf{p})$ is clearly not.

In general a scattering process with a momentum transfer $\hbar\mathbf{q}$ and energy transfer $\hbar\omega$ is described by the dynamic structure factor $S(\mathbf{q}, \omega)$. Relevant here then is the Compton, or equivalently the high-energy and momentum transfer, limit (neglecting vertex corrections), i.e.,[39]

$$S(\mathbf{q}, \omega) = \frac{1}{\rho\pi} \int_{\mu-\hbar\omega}^{\mu} \frac{d\epsilon}{2\pi} \int \frac{d^3\mathbf{p}}{(2\pi)^3} A(\mathbf{p}, \epsilon) A(\mathbf{p}+\hbar\mathbf{q}, \epsilon+\hbar\omega) \tag{2.5}$$

$$\approx \frac{1}{\rho\pi} \int \frac{d^3\mathbf{p}}{(2\pi)^3} n(\mathbf{p}) A(\mathbf{p}+\hbar\mathbf{q}, p^2/2m+\hbar\omega). \tag{2.6}$$

Here ρ is the electron density and $\hbar\omega = E_1 - E_2$ is the energy transfered to the recoil electron. In obtaining Eq. (2.6) the energy in the argument of one of the spectral density functions has been set equal to $p^2/2m$, which separates the integrals and yields the occupation number $n(\mathbf{p})$ via the low energy spectral function.[40] We emphasize that $A(\mathbf{p}, \epsilon)$ is an

asymmetric function that will generally consist of two peaks—the plasmaron and the quasiparticle peak.[6] Although this is well known in solid state theories,[38] the relevance of the shape of the spectral function has been pointed out in connection with the high-resolution Compton spectra relatively recently.[6,40]

The Compton limit to $S(\mathbf{q},\omega)$ is obtained when the spectral density function in Eq. (2.6) is replaced by a Dirac δ function. As a result, the double integral of the momentum density in the dynamic scattering factor is separated. However, the high-energy spectral density function has a finite width as a result of final-state interactions which from Eq. (2.6) may be viewed as an effective smearing of the ground-state momentum density. The size of the smearing effect will be increasingly more important at low photon energies and it may become comparable to, or even larger than, the experimental resolution. For our experiments, the approximate width (in momentum) of the final-state spectral density function was estimated to be 0.06 a.u., 0.02 a.u., and 0.006 a.u. with $E_1=10$ keV, $E_1=29$ keV, and $E_1=56$ keV, respectively.[41] These results suggest that the effective momentum resolution in low-energy Compton experiments possesses intrinsic limitations due to final-state interactions and cannot likely be enhanced arbitrarily by improving the instrumental resolution.

In this work the experimental results are compared and contrasted with the corresponding highly accurate theoretical Compton profiles and their first derivatives computed within the LDA–based band theory framework. The calculations use the all-electron charge self-consistent Korringa-Kohn-Rostoker (KKR) methodology.[42–45] The crystal potential is based on the von Barth–Hedin local density approximation[46] and is assumed to possess a nonoverlapping muffin-tin form. The band structure problem was solved to a high degree of self-consistency for the hcp Be lattice with lattice constants $a=4.3289$ a.u. and $c=6.7675$ a.u. Using the converged crystal potential, the electronic wave functions and energy bands were then obtained over 1800 *ab initio* **k** points in the irreducible 1/24th of the Brillouin zone (BZ). From these basic results, the momentum density, the Compton profiles, and their first derivatives along the three high-symmetry directions were computed over the range 0.0–5.0 a.u. on a momentum mesh of 0.01 a.u. The computations are estimated to be accurate to about one part in 10^3, so that the fine structure in the spectra can be delineated properly. The exchange-correlation effects are approximated using the isotropic LDA correction[33]

$$\Delta N^{\mathrm{LDA}}(p)=\int \rho(\mathbf{r})[N(p,\rho(\mathbf{r}))-N_0(p,\rho(\mathbf{r}))]d\mathbf{r}, \tag{2.7}$$

where $N(p,\rho(\mathbf{r}))$ and $N_0(p,\rho(\mathbf{r}))$ are the momentum densities for the interacting and noninteracting homogeneous electron gas, respectively, evaluated at the local electron density $\rho(\mathbf{r})$ of the physical system. Form (2.7) obviously does not account for the anisotropy of the electron density in crystalline materials; it also does not describe properly the correlation effects if the charge density varies rapidly.

III. EXPERIMENT

The experiments were carried out at the beam lines ID15B and ID16 of the European Synchrotron Radiation Facility (ESRF). The pertinent details of these two sets of measurements are as follows.

At beam line ID16, the radiation from two 42-period undulators was monochromatized with a two-bounce Si(111) channel-cut crystal, and the intensity of the scattered photons was measured with a crystal spectrometer operating in a Rowland geometry. The scattering angle was 165° and a spherically bent Si(555) analyzer crystal was used to measure the intensity of the scattered photons at a fixed energy $E_2=9.9$ keV. We tuned the incident rather than the scattered photon energy in order to keep the analyzer in a backscattering geometry (Bragg angle 86°), and to avoid uncertainties related to the analyzer crystal reflectivity. This approach also possesses the advantage that the scattered x-ray intensity does not need to be corrected for absorption in air, Kapton windows, etc., since these factors remain unchanged during the entire experiment. In order to account for changes in the photon flux with time (due to the storage ring electron beam decay and instability) and incident energy (due to the spectrum of the undulators and the monochromator reflectivity), the incident intensity was monitored with a Si PIN diode that detected scattered x rays from a Kapton foil placed in the incident beam at an angle of 45°. Because the energy bandwidth of the undulator radiation is relatively narrow, the undulator gaps had to be changed ~ 40 times within the region from -1.4 to 1.4 a.u. Each gap change corresponded to a 10 eV change in energy. Furthermore, special care was required with respect to the spatial distribution of the undulator radiation since this constitutes the effective source for the analyzer crystal. At the high-energy side of the undulator harmonic peak, for example, the x-ray beam splits into two vertically separated spots, which obliged us to operate on the lower-energy side only.

The momentum resolution in the measurements at beam line ID16 was $\Delta p_z \approx 0.02$ a.u. The energy bandwidth of the incident beam was 1.5 eV, where the most important factor was the Darwin width of the Si(111) monochromator crystal. The resolution of the spectrometer was about 0.35 eV, determined mainly by the source size (i.e., beam size at the sample). The uncertainty of the scattering angle (1.5°) was due to the finite size of the analyzer crystal. This was also the dominant contribution to the momentum resolution. The exact form of the instrument function was calculated via ray tracing, which yielded a slightly asymmetric function with a full width at half maximum (FWHM) of 0.02 a.u. The Compton profiles were measured with the scattering vector of the elastically scattered photons along three main crystallographic directions, namely $[10\cdot0]||\Gamma M$, $[11\cdot0]||\Gamma K$, and $[00\cdot1]||\Gamma A$. The samples were in the shape of 2.8-mm disks with a diameter of 20 mm with surface normals along the aforementioned directions. The total number of counts collected at the Compton peak at a count rate of 4000 counts/s were 2.2×10^5 ($\mathbf{q}||[10\cdot0]$), 3.0×10^5 ($\mathbf{q}||[11\cdot0]$) and 5.5×10^5 ($\mathbf{q}||[00\cdot1]$). The related statistical inaccuracies are 0.2%, 0.2%, and 0.1%, respectively. The ID16 spectrometer thus provides a very-high-momentum resolution, but it is limited to low incident photon energies. On the other hand,

this allows us to study effects due to the finite width of the high-momentum spectral density function and the failure of the impulse approximation.

At beam line ID15, the radiation source was an asymmetric multipole wiggler. The x rays were monochromatized with a horizontally bent Si crystal with a 5:1 demagnification ratio. Here we used constant incident photon energies of 29 keV and 56 keV using Si(111) and Si(311) monochromators, respectively. The Compton profiles were measured along the three high-symmetry directions ([10·0], [11·0], and [00·1]) using a scanning Rowland spectrometer with Si(400) (29 keV) and Ge(440) (56 keV) analyzer crystals. The construction and performance of the spectrometer have been recently described by Suortti *et al.*[47] The Be single crystal samples were in the shape of long sticks with a 1 mm$\times$1 mm square cross section. Only two separate samples were needed, because we could align the scattering vector parallel to [11·0] and [10·0] directions by turning the same sample by 90° without affecting the geometry due to the hexagonal symmetry.

For the 29-keV measurement, the energy bandwidth of the incident radiation due to the bending of the monochromator was $\Delta E_1 \approx 10$ eV. The resolution of the spectrometer, dominated by the effective volume of the sample, was $\Delta E_2 \approx 30$ eV, and the uncertainty of the scattering angle due to the finite size of the analyzer crystal was $\Delta\phi \approx 0.2°$. The overall momentum resolution was $\Delta p_z \approx 0.08$ a.u. The corresponding parameters for the 56-keV experiment were $\Delta E_1 \approx 40$ eV, $\Delta E_2 \approx 100$ eV, and $\Delta\phi \approx 0.3°$. The overall momentum resolution was $\Delta p_z \approx 0.16$ a.u. At the Compton peak we collected altogether 7.0×10^5 ($E_1 = 56$ keV) and 6.2×10^5 ($E_2 = 29$ keV) counts in all crystal directions, which resulted in a statistical inaccuracy of 0.1%. The count rates at the Compton peak were 3000 counts/s ($E_1 = 29$ keV) and 3500 counts/s ($E_1 = 56$ keV).

In all experiments, the spectra were measured independently several times, and the individual spectra were summed using the associated statistical accuracy as a weight. The difference between each spectrum and the sum of the spectra were found to be statistically consistent in all cases. A linear background of approximately 0.4% of $J(0)$ on the energy scale was determined by assuming that the far-extending tails of the measured profiles must represent the pure core electron contribution.

Equation (2.2) makes it obvious that the Compton profile of any system should be symmetric with respect to $p_z = 0$. However, the profiles extracted from the experimental data are well known to display asymmetry due to the failure of the impulse approximation and multiple scattering events. Furthermore, at low photon energies ($\sim$10 keV), the valence electron contribution can become asymmetric to an extent even larger than for the core electrons.[48] The experimental core Compton profile is slightly asymmetric even when the incident energy is of the order of 50 keV. We have extracted this asymmetry from the experimental high-energy ($E_1 = 29$ keV and 56 keV) data and found it to be close to the results of a calculation based on hydrogenic wave functions for the core electrons.[13] The maximum asymmetry is about 1% of $J(0)$, and varies very slowly with momentum. Accordingly, we smoothed the extracted asymmetry and subtracted it from the directional profiles. A symmetrization method used more often is to average the negative and positive sides of the Compton profiles. However, the method used here has the advantage that the positive and the negative sides of our final (symmetric) profiles involve uncorrelated data. This can be very useful in establishing the existence of a subtle feature in the data by confirming its presence in two independent locations. A systematic study of the core asymmetry will be published elsewhere.[49] In the case of low-energy experiments ($E_1 = 10$ keV), the valence electron contribution also shows asymmetry and exhibits directional dependence, making it difficult to determine a smooth asymmetric subtraction. Therefore no asymmetry correction was applied to the 10-keV data.

Multiple scattering effects were assessed via extensive Monte Carlo calculations,[50] which suggest that for the high-energy measurements ($E_1 = 29$ keV and 56 keV), the multiple scattering contribution is only about 2% of the integrated area of the Compton profile. The associated maximum asymmetry is found to be only 0.1%, which is much less than the observed value due to the core asymmetry.

IV. RESULTS AND DISCUSSION

Figure 1 presents the normalized experimental Compton profiles measured with various energies along three main crystallographic directions, together with the corresponding resolution-broadened KKR calculations including the Lam-Platzman correction. The unbroadened theoretical profiles are also shown for reference. The agreement between theory and experiment with respect to the overall shapes of the profiles along all three directions and at each of the three photon energies considered is seen to be remarkably good. Note that the present LDA band theory framework of course does not involve the photon energy. The theoretical profiles shown for various photon energies differ only in the amount of broadening used to reflect the experimental resolution. Our definition of p_z follows that of Holm,[51] where the positive values of p_z correspond to the high-energy side of the Compton profile. One can clearly see how the different directions have significantly distinct Compton profiles due to the hexagonal crystal structure and the relatively complicated Fermi surface of beryllium. A glitch originating from multiple Bragg diffraction in the sample was observed very close to the peak as well as at $p_z = 0.5$ a.u. in the [10·0] profile of the 10-keV experiment, which gives some uncertainty to this profile, especially at the Compton peak. The profiles with $E_1 = 29$ keV and $E_1 = 56$ keV are normalized to the same area as the theoretical profiles between -5 and 5 a.u. The profiles with $E_1 = 10$ keV are normalized only between -4 and 1 a.u. due to the K edge of the $1s$ electrons (112 eV). The edge is clearly visible in the low-energy profiles at $p_z = 1.9$ a.u. The fact that the theory and experiment continue to show good accord in Fig. 1 even at the low photon energy suggests that the possible breakdown of the impulse approximation at 10 keV in Be does not appear to influence the shape of the profile substantially.

Previous experiments[5,6,22] have shown that the peak height of the experimental Compton profiles is lower than predicted by the theory. This is also the result of the present experiment, although now the agreement between theory and experiment is slightly better. Generally, effects of multiple

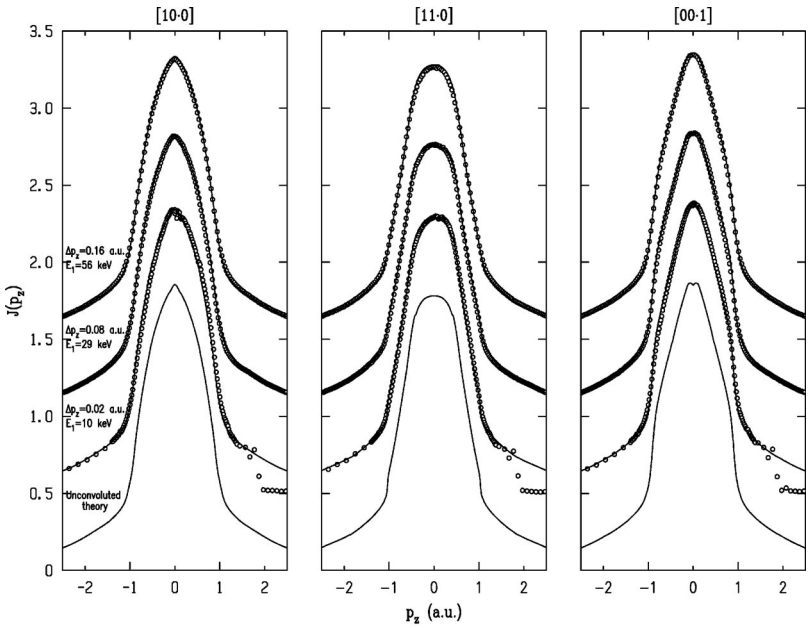

FIG. 1. Experimental and theoretical directional Compton profiles with the scattering vector along [10·0], [11·0], and [00·1] directions, measured at three different energies. Values of the photon energy (E_1) and the corresponding momentum resolution (Δp_z) are given in the left-hand side panel. Open circles give the experimental points; the error bars are smaller than the symbol size. Solid lines represent the theoretical profiles based on the local density approximation, which are convoluted with the appropriate experimental resolution. For comparison, the unconvoluted theoretical profile is shown at the bottom of each panel.

scattering, background subtraction, and detector dead time corrections, for example, can change the Compton profile peak value. In view of these experimental uncertainties, caution should be exercised in adducing correlation effects on the basis of the peak heights in the Compton data.

In order to expose the fine structure, which is due to the complicated Fermi surface topology of Be, it is convenient to study the derivatives of the Compton profiles. Figure 2 presents the first derivatives of the measured directional Compton profiles for various photon energies and crystallographic directions. We emphasize that the experimental derivatives here have been obtained via a direct numerical differentiation without using filtering procedures invoked in previous studies to smooth noise.[5,22] Figure 2 shows the excellent level of detail at which the theory reproduces fine spectral features in the data and the importance of experimental resolution in this connection. Comparing the data sets we see that the improvement of the resolution by a factor of 2 makes an important change between the 56-keV and 29-keV data, which can be seen as a sharpening of structure and appearance, for example, of the Fermi surface peak around 1 a.u. in the 29-keV [11·0] profile.

In Fig. 2 several features arising from the Fermi surface topology can be identified.[5,22] This is done most easily with reference to the unbroadened theory curves in Fig. 2. Recall that the Fermi surface of Be consists of a coronet-shaped hole surface in the second Brillouin zone and a cigar-like electron surface in the third zone.[52] The contributions of these sheets are seen in the derivatives of the directional Compton profiles. The details are perhaps richest in the [11·0] direction, where two cigars are projected on to the scattering vector at $p_z = 0.4$ a.u., giving rise to a maximum. At $p_z = 0.6$ a.u. the integration is over the large holelike coronet, and the momentum density decreases rapidly, as indicated by a sharp drop in the derivative. The Fermi surface is reached at $p_z = 1.0$ a.u., and a cigar is traversed, as

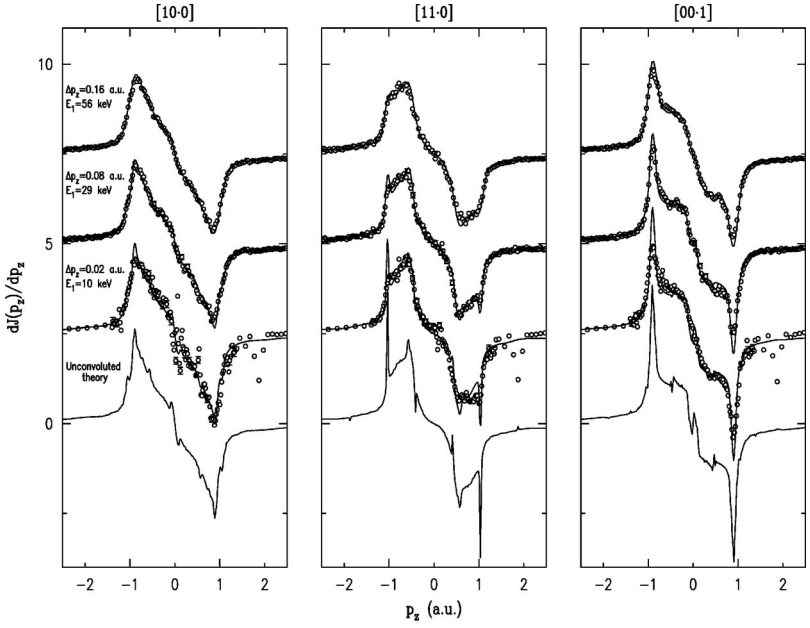

FIG. 2. Same as the caption to Fig. 1, except that this figure refers to the first derivatives of the various experimental and resolution broadened Compton profiles in order to highlight the fine structure in the data. For clarity, error bars are drawn for every fifth point and even then only if they are larger than the symbol size. Various structural features are discussed in the text.

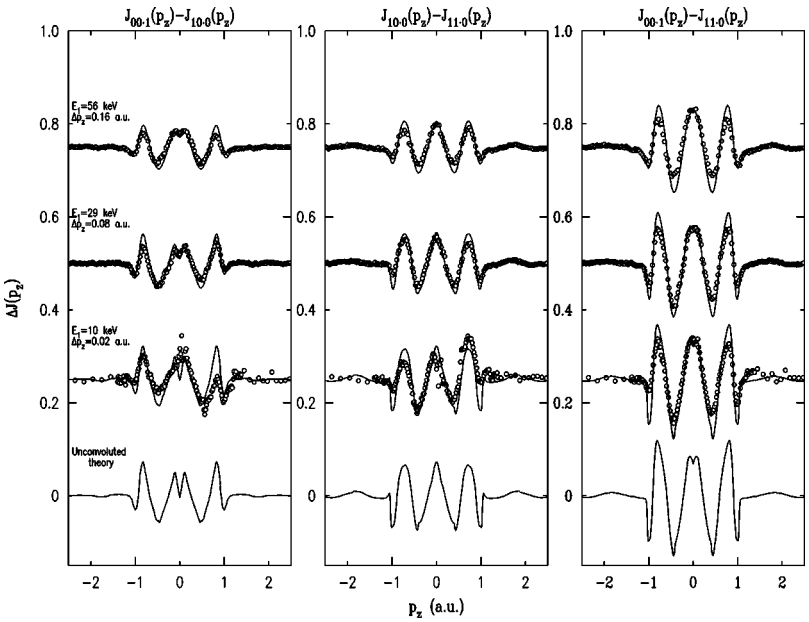

FIG. 3. Same as the caption to Fig. 1, except that this figure refers to anisotropies in the theoretical and experimental profiles defined as differences between various pairs of directional Compton profiles. The specific difference involved is indicated on the top of each panel. The error bars are smaller than the symbol size.

seen in a steep decrease of the derivative. In the $[10\cdot0]$ direction the integration plane traverses two cigars at $p_z=0$ a.u., and their edges are seen as a sharp change of the derivative. Unfortunately, due to a multiple Bragg reflection ''glitch'' near $p_z=0$ a.u., we cannot say whether the feature would be visible in the 10-keV data. There is a small feature at $p_z=0.6$ a.u. due to the coronet, which is visible in the high-resolution data. The Fermi surface is reached at $p_z=0.9$ a.u., and the momentum density falls off rapidly. Finally, the $[00\cdot1]$ data shows three sharp features. The distance between the two sharp edges at $p_z=0$ a.u. and $p_z=0.5$ a.u. corresponds to the vertical dimension of the cigars. There is no Fermi surface in this direction, but the drop at $p_z=0.9$ a.u. is caused by the surface of the second Brillouin zone. Most of the aforementioned features can be more or less seen in the experimental spectra of Fig. 2.

Despite a wide-ranging level of agreement between theory and experiment in Fig. 2, it is striking that the theoretically predicted sharpening of the Fermi surface dip around 1 a.u. in the $[11\cdot0]$ spectrum, even when the instrumental resolution improves by a factor of 4 in going from 29 keV (resolution 0.08 a.u.) to 10 keV (resolution 0.02 a.u.), is not observed in the measurements. As already noted, the width of the high-momentum spectral density function in Eq. (2.6) acts to smear the momentum density. The associated FWHM is estimated to be 0.06 a.u. at 10 keV and 0.02 a.u at 29 keV; if so, this effect will dominate the instrumental resolution at 10 keV but not at 29 keV, and explain why the improved instrumental resolution at 10 keV does not lead to significantly sharper Fermi surface features in the data. In addition, the spectral density function consists of two Lorenzian peaks and thus the smearing effect is generally slightly larger than given by the FWHM. This broadening effect has been noted previously in Li in Ref. 6 where the breakdown of the impulse approximation at low photon energies below 10 keV is implicated. A more recent discussion of Li in terms of the final-state interactions involving the high-energy spectral density function is provided elsewhere.[53] There are more subtle effects related to the inadequacy of the Lam-Platzman correction in incorporating correlation effects in the theory, but we will return to this point in connection with Fig. 4 below.

Figure 3 compares theoretical and experimental anisotropies by taking differences between various pairs of directional Compton profiles. Since the isotropic parts of the profiles are subtracted in this way, the results of Fig. 3 are insensitive to various experimental contributions, which are uncertain but largely isotropic (e.g., core spectra and their asymmetries, multiple scattering corrections, etc.). The excellent agreement between theory and experiment seen in Fig. 3 with respect to the amplitudes as well as various structural details is striking. This, however, is not surprising since this is consistent with the results of Figs. 1 and 2. Amplitudes of the theoretical anisotropies are generally slightly larger than the experimental values, although the discrepancies are smaller than in previous experiments.[5,22] This observation is well understood on the basis of the previously discussed differences in the derivatives, which are also reflected in the anisotropies. The discrepancies for the 10-keV data are larger, especially where the $[10\cdot0]$ directional profile is involved in taking the differences. This is mostly due to the asymmetry of valence electron profiles, which also exhibits directional dependence. In this case, the valence electron profile asymmetry is induced by the spectral function correction and vertex corrections[48] (see Sec. III). For the 29-keV as well as 56-keV measurements, the anisotropy in Fig. 3 is seen to be essentially symmetric; this confirms that the asymmetries in the two high-energy profiles arise from the core and not the valence electrons. In contrast, the 10-keV data in Fig. 3 are visibly asymmetric, indicating the involvement of valence electrons in this case. As already seen before in Fig. 2, the 10-keV data do not reveal any finer details as expected on the basis of a better momentum resolution.

Figure 4 presents the residual differences between the experimental and theoretical Compton profiles for the 56-keV measurements. The theoretical profiles used here include the isotropic Lam-Platzman correction and have been broadened to reflect the effective instrumental resolution (as noted above, the broadening introduced via final-state effects at 56 keV of ~ 0.006 a.u. is negligible). Note that the differences

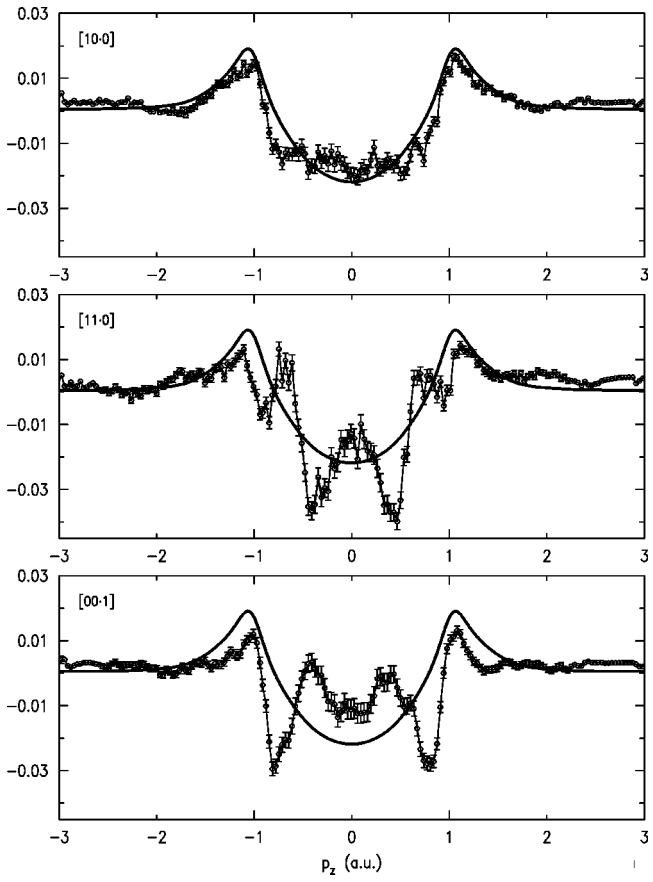

FIG. 4. Absolute differences (open circles) between the experimental and Lam-Platzman corrected theoretical Compton profiles with $E_1=56$ keV along the three high-symmetry directions. The theoretical profiles are broadened with the experimental instrument function before subtraction. The thick solid line represents the Lam-Platzman correction. The thin solid line is a guide to the eye through the data points.

of Fig. 4 are of order 1% of the profiles and for this reason are difficult to see in Fig. 1, but are more visible in the derivative spectra of Fig. 2 or the anisotropy plots of Fig. 3. The Lam-Platzman correction itself is shown for comparison (solid line), and it is of course the same along the three directions due to its isotropy; it is clearly seen that the amplitude as well as the overall momentum dependence of the residuals in Fig. 4 are well mimicked by the Lam-Platzman curve. In fact, along $[10\cdot0]$ (top panel) where the residuals possess relatively little fine structure, an *ad hoc* scaling of the Lam-Platzman correction included in the theory by a factor of 2 will bring theory and experiment into an essentially perfect agreement at all momenta. However, the residuals of Fig. 4 display a substantial directional dependence as well as seen from the middle and lower panels. The peculiar sharper features along $\mathbf{q}||[11\cdot0]$ and $\mathbf{q}||[00\cdot1]$, which lie well outside the error bars of the data, may be associated with the structure of the Fermi surface, especially the location of the Fermi surface cigars. The failure of the isotropic Lam-Platzman correction is most evident in these cases. On the other hand, along the $[10\cdot0]$ direction the Fermi surface cigars are not traversed until near the *M* points in the first Brillouin zone, and there is rather little fine structure in the difference between experiment and theory. In short, the systematic nature of the discrepancies in Fig. 4 suggests that the standard LDA-based description of the ground-state momentum density is not adequate in Be, and that theoretical schemes for a proper treatment of correlation effects in the inhomogenous electron gas need to be developed in order to understand the Compton spectra of solids.

V. SUMMARY AND CONCLUSIONS

We report high-resolution Compton profiles of Be single crystals using three different incident photon energies of 10 keV, 29 keV, and 56 keV along each of the three main crystallographic directions ($[10\cdot0]$, $[11\cdot0]$, and $[00\cdot1]$), together with corresponding highly accurate computations based on the LDA band theory framework. The momentum resolution in our measurements varies from 0.02 a.u. at 10 keV to 0.08 a.u. at 29 keV and 0.16 a.u. at 56 keV, enabling a systematic study of the effects of incident energy dependence and momentum resolution in the experimental Compton spectra. Extensive comparisons reveal an excellent level of agreement between theoretical predictions and the measurements in almost all cases. The agreement extends to the shapes of the directional profiles; the evolution of much of the fine structure in the first derivatives of the profiles with increasing momentum resolution; and the amplitude as well as the structure in the anisotropies defined as differences between various pairs of directional profiles. Based on these results, high-resolution Compton scattering is concluded to be a useful tool in Fermi surface studies. Many fine details of the Fermi surface can be revealed especially in the derivatives of the experimental Compton profiles, which can be easily associated with the Fermi surface topology.

The measured profiles at 10 keV exhibit a broadening of the fine structure in the data that is greater than that expected on the basis of the instrumental resolution function, even though this is not the case at 29-keV or 56-keV incident photon energies. A similar effect has been observed in Li, where it may be explained in terms of the breakdown of the impulse approximation at low photon energies.[53] The final-state interactions can then be modeled approximately as an effective smearing of the momentum density; the associated momentum smearing in the case of Be is estimated to be 0.06 a.u., 0.02 a.u., and 0.006 a.u. with $E_1=10$ keV, $E_1=29$ keV, and $E_1=56$ keV, respectively.[41] These results suggest that the effective momentum resolution in low-energy Compton experiments possesses intrinsic limitations due to final-state interactions and possibly cannot be enhanced arbitrarily by improving the instrumental resolution. Finally, we note that even at the high photon energy of 56 keV where final-state effects are negligible, small but systematic discrepancies between the theory and experiment at the level of order 1% of the profiles remain. These discrepancies are direction dependent and possess fine structure well above the experimental error bars, indicating that the LDA-based framework with an isotropic Lam-Platzman correction, implicit in our theoretical approach, is not adequate and that a better treatment of the electron correlation effects in the inhomogeneous electron gas is needed to develop a satisfactory description of the momentum density in Be.

ACKNOWLEDGMENTS

We would like to acknowledge J. Schneider for the Be single crystal specimens used at ID16, and F. Sette, M. Krisch, A. Soininen, W. Schülke, and B. Barbiellini for invaluable discussions. This work was supported by the Academy of Finland (7379/40732), the U.S. Department of Energy under Contract No. W-31-109-ENG-38, a travel grant from NATO, and benefited from the allocation of supercomputer time at the NERSC and the Northeastern University Advanced Scientific Computation Center (NU-ASCC).

*Permanent address: Academy of Mining and Metallurgy, Cracow, Al. Mickiewicza 30, Poland.

[1] M.J. Cooper, Rep. Prog. Phys. **48**, 415 (1985).

[2] A. Bansil, Z. Naturforsch. Teil A **48A**, 165 (1993).

[3] S. Manninen, J. Phys. Chem. Solids **61**, 335 (2000).

[4] Y. Sakurai, Y. Tanaka, A. Bansil, S. Kaprzyk, A.T. Stewart, Y. Nagashima, T. Hyodo, S. Nanao, H. Kawata, and N. Shiotani, Phys. Rev. Lett. **74**, 2252 (1995).

[5] K. Hämäläinen, S. Manninen, C.-C. Kao, W. Caliebe, J.B. Hastings, A. Bansil, S. Kaprzyk, and P.M. Platzman, Phys. Rev. B **54**, 5453 (1996).

[6] W. Schülke, G. Stutz, F. Wohlert, and A. Kaprolat, Phys. Rev. B **54**, 14 381 (1996).

[7] G. Stutz, F. Wohlert, A. Kaprolat, W. Schülke, Y. Sakurai, Y. Tanaka, M. Ito, H. Kawata, N. Shiotani, S. Kaprzyk, and A. Bansil, Phys. Rev. B **60**, 7099 (1999).

[8] A. Bansil, S. Kaprzyk, A. Andrejczuk, L. Dobrzynski, J. Kwiatkowska, F. Maniawski, and E. Zukowski, Phys. Rev. B **57**, 314 (1998).

[9] Y. Sakurai, S. Kaprzyk, A. Bansil, Y. Tanaka, G. Stutz, H. Kawata, and N. Shiotani, J. Phys. Chem. Solids **60**, 905 (1999).

[10] P. Eisenberger and P.M. Platzman, Phys. Rev. B **2**, 415 (1970).

[11] A. Issolah, Y. Garreau, B. Levy, and G. Loupias, Phys. Rev. B **44**, 11 029 (1991).

[12] A. Issolah, B. Levy, A. Beswick, and G. Loupias, Phys. Rev. A **38**, 4509 (1988).

[13] P. Holm and R. Ribberfors, Phys. Rev. A **40**, 6251 (1989).

[14] R.K. Pathak, A. Kshirsagar, R. Hoffmeyer, and A.J. Thakkar, Phys. Rev. A **48**, 2946 (1993).

[15] P.M. Bergstrom, T. Suric, K. Pisk, and R.H. Pratt, Phys. Rev. B **48**, 1134 (1993).

[16] P.P. Kane, Phys. Rep. **218**, 67 (1992).

[17] J. Laukkanen, K. Hämäläinen, and S. Manninen, J. Phys.: Condens. Matter **8**, 2153 (1996).

[18] L. Dobrzynski and A. Holas, Nucl. Instrum. Methods Phys. Res. A **383**, 589 (1996).

[19] Y. Tanaka, N. Sakai, and H. Kawata, Phys. Rev. Lett. **70**, 1537 (1993).

[20] P. Suortti, T. Buslaps, V. Honkimäki, C. Metz, A. Shukla, Th. Tschentscher, J. Kwiatkowska, F. Maniawski, A. Bansil, S. Kaprzyk, A.S. Kheifts, D.R. Lun, T. Sattler, J.R. Schneider, and F. Bell, J. Phys. Chem. Solids **61**, 397 (2000).

[21] I. Matsumoto, J. Kwiatkowska, F. Maniawski, S. Kaprzyk, A. Bansil, M. Itou, H. Kawata, and N. Shiotani, J. Phys. Chem. Solids **61**, 375 (2000).

[22] M. Itou, Y. Sakurai, T. Ohata, A. Bansil, S. Kaprzyk, Y. Tanaka, H. Kawata, and N. Shiotani, J. Phys. Chem. Solids **59**, 99 (1998).

[23] S. Berko, in *Compton Scattering*, edited by B.G. Williams (McGraw-Hill, London, 1977); P.E. Mijnarends and A. Bansil, in *Positron Spectroscopy of Solids*, edited by A. Dupasquier and A.P. Mills, Int. School of Physics ''Enrico Fermi'' ISO Press, Amsterdam, 1995), pp. 257–274.

[24] A. Bansil and S. Kaprzyk, Mater. Sci. Forum **255-257**, 129 (1997).

[25] *Compton Scattering*, edited by B.G. Williams (McGraw-Hill, London, 1977).

[26] E. Daniel and S.H. Vosko, Phys. Rev. **120**, 2041 (1960).

[27] L. Hedin and S. Lundqvist, Solid State Phys. **23**, 1 (1969).

[28] J. Lam, Phys. Rev. B **3**, 3243 (1971).

[29] L.J. Lantto, Phys. Rev. B **22**, 1380 (1980).

[30] A.W. Overhauser, Phys. Rev. B **3**, 1888 (1971).

[31] Y. Takada and H. Yasuhara, Phys. Rev. B **44**, 7879 (1991).

[32] E. Pajanne and J. Arponen, J. Phys. C **15**, 2683 (1982).

[33] L. Lam and P.M. Platzman, Phys. Rev. B **9**, 5122 (1974).

[34] B. Kralik, P. Delaney, and S.G. Louie, Phys. Rev. Lett. **80**, 4253 (1998).

[35] C. Filippi and D.M. Ceperley, Phys. Rev. B **59**, 7907 (1999).

[36] B. Barbiellini, J. Phys. Chem. Solids **61**, 341 (2000).

[37] A.G. Eguiliz, W. Ku, and J.M. Sullivan, J. Phys. Chem. Solids **61**, 383 (2000).

[38] G.D. Mahan, *Many Particle Physics* (Plenum, New York, 1981).

[39] T.K. Ng and B. Dabrowski, Phys. Rev. B **33**, 5358 (1986).

[40] Y. Kubo, J. Phys. Soc. Jpn. **65**, 16 (1996).

[41] A. Soininen (private communication).

[42] A. Bansil and S. Kaprzyk, Phys. Rev. B **43**, 10 335 (1991).

[43] S. Kaprzyk and A. Bansil, Phys. Rev. B **42**, 7358 (1990).

[44] A. Bansil, S. Kaprzyk, and J. Toboła, in *Application of Multiple Scattering Theory in Material Science*, edited by W. H. Butler *et al.*, MRS Symposia Proceedings No. 253 (Materials Research Society, Pittsburgh, 1992), p. 505.

[45] A. Bansil, S. Kaprzyk, P.E. Mijnarends, and J. Tobola, Phys. Rev. B **60**, 13 396 (1999).

[46] U. von Barth and L. Hedin, J. Phys. C **5**, 1629 (1972); A.K. Rajagopal and J. Callaway, Phys. Rev. B **7**, 1912 (1973).

[47] P. Suortti, T. Buslaps, P. Fajardo, V. Honkimäki, M. Kretzschmer, U. Lienert, J.E. McCarthy, M. Renier, A. Shukla, T. Tschentscher, and T. Meinander, J. Synchrotron Radiat. **6**, 69 (1999).

[48] W. Schülke (private communication).

[49] S. Huotari *et al.* (unpublished).

[50] V. Honkimäki (private communication).

[51] P. Holm, Phys. Rev. A **37**, 3706 (1988).

[52] T.H. Loucks and P.H. Cutler, Phys. Rev. **133**, A819 (1964).

[53] C. Sternemann *et al.*, Phys. Rev. B (to be published).